Scanned-wavelength-modulation spectroscopy near 2.5 μm for H_2O and temperature in a hydrocarbon-fueled scramjet combustor

C. S. Goldenstein · I. A. Schultz · R. M. Spearrin · J. B. Jeffries · R. K. Hanson

Abstract The design and demonstration of a two-color tunable diode laser sensor for measurements of temperature and H_2O in an ethylene-fueled model scramjet combustor are presented. This sensor probes multiple H_2O transitions in the fundamental vibration bands near 2.5 μm that are up to 20 times stronger than those used by previous near-infrared H_2O sensors. In addition, two design measures enabled high-fidelity measurements in the nonuniform flow field. (1) A recently developed calibration-free scanned-wavelength-modulation spectroscopy spectral-fitting strategy was used to infer the integrated absorbance of each transition without a priori knowledge of the absorption lineshape and (2) transitions with strengths that scale near-linearly with temperature were used to accurately determine the H_2O column density and the H_2O-weighted path-averaged temperature from the integrated absorbance of two transitions.

1 Introduction

Over the past two decades, tunable diode laser absorption spectroscopy (TDLAS) has matured into a robust technique for providing time-resolved, species-specific measurements of gas temperature, composition, pressure, and velocity in a wide range of practical applications [1–3]. More specifically, TDLAS sensors have been used in internal combustion engines [4–6], pulsed detonation combustors [7–

11], scramjets [12–17], gas turbines [18, 19], and to provide 2D temperature and H_2O measurements [20]. Here, temperature and H_2O measurements were acquired in the University of Virginia's dual-mode scramjet combustor as part of the National Center for Hypersonic Combined Cycle Propulsion's (NCHCCP) effort to characterize and model several scramjet combustor configurations. Although the basic principles of a scramjet engine are simple, a number of complex phenomena (e.g., shock-boundary-layer interactions, turbulence, and chemical kinetics) continue to hinder scramjet development. Hydrocarbon-fueled systems pose even greater challenges due to their complex and comparatively slow chemistry. As a result, tunable diode laser (TDL) sensors continue to play a vital role in providing critical information regarding the combustion and flow physics governing these devices.

While considerable sensing of H_2O has been conducted in scramjets [12–14, 16, 17], all of that work was conducted using the weaker near-infrared (NIR) overtone and combination bands ($2v_1$ and $v_1 + v_3$). By using the H_2O fundamental vibration bands, the sensor reported here realizes three primary benefits: (1) access to lines that are up to 20 times stronger than overtone and combination band lines, (2) access to strong lines with larger lower-state energy for increased temperature sensitivity and improved measurement fidelity in high-temperature nonuniform flows [21], and (3) reduced Doppler broadening due to the longer wavelengths used which leads to larger peak absorbance and WMS signals. These three benefits improve the accuracy, precision, and sensitivity of TDLAS sensors, and therefore, enable study of a greater range of applications.

We present the design and demonstration of a two-color TDLAS sensor for highly sensitive measurements of temperature and H_2O near 2.5 μm. The sensor was designed and validated at Stanford University and then deployed at

C. S. Goldenstein (✉) · I. A. Schultz · R. M. Spearrin · J. B. Jeffries · R. K. Hanson
High Temperature Gasdynamics Laboratory, Department of Mechanical Engineering, Stanford University, Stanford, CA 94305, USA
e-mail: csgolden@stanford.edu

the University of Virginia's Supersonic Combustion Facility (UVaSCF). Measurements were acquired along more than 35 lines-of-sight (LOS) within the combustor to characterize the combustion process. This sensor used two frequency-multiplexed fiber-coupled TDLs near 2,551 and 2,482 nm to probe three H_2O transitions with lower-state energies of 704, 2,660, and 4,889 cm^{-1}. Two design measures enabled high-fidelity measurements in the non-uniform reaction zone: (1) a recently developed first-harmonic-normalized scanned-wavelength-modulation spectroscopy with second-harmonic-detection (scanned-WMS-2f/1f) spectral-fitting strategy was used to infer the integrated absorbance of each transition without prior knowledge of the transition linewidths and (2) transitions with strengths that scale near-linearly with temperature were used to accurately determine the H_2O column density and the H_2O-weighted path-averaged temperature from the integrated absorbance of two transitions [21].

2 Experimental setup

2.1 University of Virginia Supersonic Combustion Facility (UVaSCF)

The UVaSCF, shown in Fig. 1, is an electrically heated, continuous-flow wind tunnel designed to produce flow conditions encountered by hypersonic aircraft. In the current study, the total temperature, total pressure, and Mach number at the combustor inlet were 1,200 K, 330 kPa, and 2, respectively. This configuration consists of four main sections: (1) isolator, (2) combustor, (3) constant area section, and (4) extender. The isolator is 3.81 cm deep (z-direction) and 2.54 cm wide (y-direction). The combustor flow path is 3.81 cm deep and diverges at 2.9° along
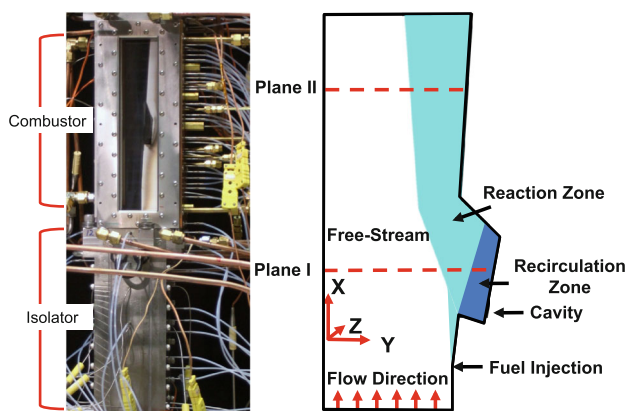

Fig. 1 Photo of UVaSCF (*left*) and cartoon of combustor with labeled measurement planes (*right*). Line-of-sight measurements were acquired in the z-direction through the large windows shown in the photo

the cavity flameholder wall. The cavity is 0.9 cm wide and 4.73 cm long. Ethylene was injected 2.46 cm upstream of the cavity at five coplanar injection sites that span the depth of the combustor. Downstream of the combustor, the flow path consisted of a 14.9-cm-long constant area section and a 18-cm-long extender which was open to the atmosphere.

2.2 TDLAS sensor hardware

A schematic of the optical setup used for temperature and H_2O measurements in the UVaSCF is shown in Fig. 2. Two frequency-multiplexed TDLs (Nanoplus GmbH) near 2,551 and 2,482 nm were used to probe H_2O transitions near 3,920, 4,029.5, and 4,030.7 cm^{-1}. During a given experiment, the transition near 3,920 cm^{-1} was probed simultaneously with either the transition near 4,029.5 cm^{-1} or the transition near 4,030.7 cm^{-1}. Each laser produced a nominal power output of 1–5 mW and a linewidth less than 3 MHz [22]. The lasers were injection-current tuned with a scanning sinusoid at 250 Hz (giving a measurement repetition rate of 500 Hz) and a modulation sinusoid at 75 or 100 kHz. A modulation depth of 0.16–0.20 and 0.031–0.038 cm^{-1} was used for the lasers at 2,551 and 2,482 nm, respectively. For both lasers, the modulation index, defined as the ratio of the modulation depth and transition half-width at half-maximum (HWHM), was between 3 and 3.5 to reduce sensitivity to potential lineshape modeling errors as recommended in [23].

A 4-mm focal length anti-reflection-coated aspheric lens (Thorlabs C036TME-D) was used to collimate the output beam of each laser. The two lasers were oriented orthogonal to one another, and a 50/50 beam splitter (Thorlabs BSW23) was used to combine the laser beams. One of the combined beam paths was directed into a 400-μm ZBLAN multi-mode fiber (Fiber-Labs) using a 6-mm focal length lens (Innovation Photonics). The fiber-coupled light was directed to the flow facility, collimated with a 20-mm focal length zinc-selenide lens, and pitched across the combustor with a near-Gaussian full-width at half-maximum (FWHM) of approximately 3 mm.

A single set of fused silica windows, shown in Fig. 1, enabled optical access throughout the combustor. Three optical filters were used to reduce detected emission. A broad band-pass filter (Spectrogon BBP-2200-2600c nm) and a long-pass filter (Spectrogon LP-2440 nm) were used to create a band-pass filter from 2,440 to 2,600 nm. In addition, a neutral density filter was used to further reduce power levels by 80 %. A 12.5-mm-diameter, 20-mm focal length calcium fluoride lens (Thorlabs LA5315-D) was used to focus the collected light onto a mercury cadmium telluride (MCT) detector (Vigo Systems PVI-2TE-4) with a 2-mm-diameter active area and 10 MHz bandwidth. The pitch and catch optics were mounted to a set of computer-controlled translation stages to traverse the measurement

Fig. 2 Schematic of optical setup used in measurements conducted at the UVaSCF
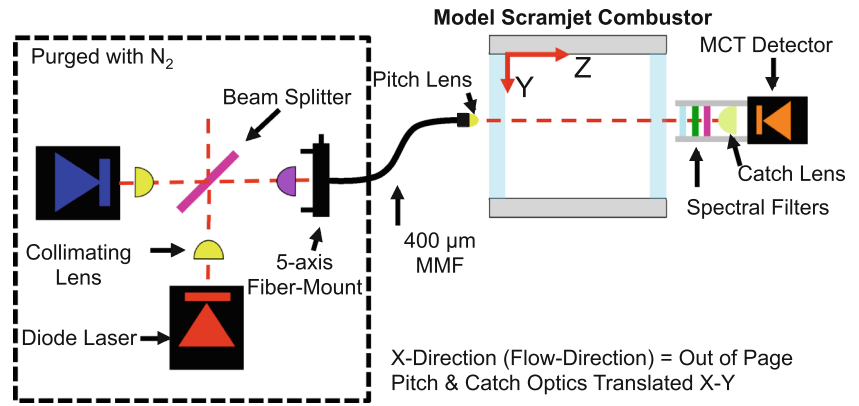
LOS in the x- and y-direction. More information regarding the arrangement of the translation stages can be found in [16]. Measurements were acquired at two axial planes (shown in Fig. 1) spaced 7.6 cm apart. The upstream-most plane was located 4.62 cm downstream of fuel injection. At each axial plane, 250 measurements (i.e., 0.5 s of data) were acquired at up to 26 different locations spaced 1.5 mm apart in the y-direction. During all experiments, the raw detector signal was anti-aliased to 1 MHz with a low-pass filter (Kronhite) and sampled at 5 MHz (National Instruments PXI-6115). The WMS signals of each laser were frequency demultiplexed during post-processing with 5-kHz Butterworth filters.

3 LOS absorption and scanned-WMS-2f/1f fundamentals

3.1 LOS absorption

Line-of-sight absorption in a nonuniform flow field is discussed in detail in [21]. As a result, only the essential fundamentals are shown here to guide the reader through the sensor design presented in Sect. 4. When the gas conditions vary along the LOS, the absorption of monochromatic light is described by the Beer–Lambert relation in path-integral form (1).

$$\frac{I_t}{I_o} = \exp[-\alpha(v)] = \exp\left[-\sum_j \int_0^L S_j(T)n_i\phi_j(v,T,P,\chi)\right]$$ (1)

Here, $\alpha(v)$ is the spectral absorbance at optical frequency v (cm^{-1}), $S_j(T)$ (cm^{-1}/molecule-cm^{-2}) is the temperature-dependent linestrength of transition j, given by (2), n_i (molecule/cm^3) is the number density of absorbing species i, ϕ_j (cm) is the lineshape function of transition j, T (K) is the gas temperature, P (atm) is the gas pressure, χ is the gas composition vector, and L (cm) is the optical path length.

$$S_j(T) = S_j(T_o)\frac{Q(T_o)}{Q(T)}\exp\left[-\frac{hcE''}{k}\left(\frac{1}{T}-\frac{1}{T_o}\right)\right]$$
$$\times \left[1-\exp\left(-\frac{hcv_o}{kT}\right)\right]\left[1-\exp\left(-\frac{hcv_o}{kT_o}\right)\right]^{-1}$$ (2)

Here, T_o (K) is the reference temperature (296 K), Q is the partition function of the absorbing molecule, taken from [24], h (J s) is Planck's constant, c (cm/s) is the speed of light, E'' (cm^{-1}) is the lower-state energy of the quantum transition, k (J/K) is the Boltzmann constant, and v_o (cm^{-1}) is the linecenter frequency of the transition.

The integrated absorbance of a single transition is given by (3).

$$A_j \equiv \int_{-\infty}^{\infty} \alpha(v)dv = \int_0^L S_j(T)n_i dl$$ (3)

If two transitions with strengths that scale linearly with temperature are used, the absorbing-species number-density-weighted path-average temperature, $\overline{T}_{n_i}$, given by (4) can be inferred by comparing the measured two-color ratio of integrated absorbances with the simulated two-color ratio of transition linestrengths [21].

$$\overline{T}_{n_i} \equiv \frac{\int_0^L Tn_i dl}{\int_0^L n_i dl} = f\left(\frac{A_2}{A_1}\right)$$ (4)

With $\overline{T}_{n_i}$ measured, the absorbing-species column density given by (5) can be calculated using (6) if the transition linestrength scales linearly with temperature [21].

$$N_i \equiv \int_0^L n_i dl$$ (5)

$$N_i = \frac{A}{S(\overline{T}_{n_i})}$$ (6)

More details regarding the determination of $\overline{T}_{n_i}$ and N_i are given in [21].

3.2 Scanned-WMS-2f/1f

WMS is a well-established TDLAS technique for measuring gas temperature and composition [25–32]. In particular, WMS-2f/1f has been widely used in a number of harsh environments [4, 10, 12, 32, 33] due to its emission- and noise-rejection benefits [29, 31, 34]. In scanned-WMS-2f/1f, one or more TDLs are each injection-current tuned with two sinusoidal signals. A slow (250 Hz here) sinusoidal scan is used to tune the nominal laser wavelength across an absorption feature, and a fast (75 or 100 kHz here) sinusoidal modulation is used to generate the WMS harmonic signals. The WMS harmonics result from the interaction between the rapidly modulated laser wavelength and the absorption lineshape. During an experiment, only the raw detector signal is acquired and the WMS harmonic signals are extracted with digital lock-in filters during post-processing [14, 15, 23, 29, 35].

Here, gas properties were calculated using the calibration-free scanned-WMS-2f/1f spectral-fitting technique developed by Goldenstein et al. [23] for two primary reasons: (1) This method does not require prior knowledge of transition linewidths and (2) this method infers the integrated absorbance of each transition which facilitates the determination of $\overline{T}_{n_i}$ and N_i. These attributes enable accurate WMS-based measurements along a line-of-sight with nonuniform composition and temperature where the transition linewidths and, therefore, lineshapes cannot be determined a priori [16, 21]. In this technique, a simulated scanned-WMS-2f/1f spectrum is least-squares fit to a measured scanned-WMS-2f/1f spectrum with the transition linecenter (v_o), integrated absorbance (A), and collisional width (Δv_c) as free parameters. The best-fit parameters are then used to calculate gas properties. Here, the Voigt profile was used to model the transition near 3,920 cm^{-1}, and the Galatry profile was used to model the transitions near 4,029.5 and 4,030.7 cm^{-1} due to their small collisional-broadening-to-narrowing ratio [36]. In all cases, the Doppler width (Δv_D) was fixed at the temperature-specified value. When using the Galatry profile, the collisional narrowing parameter was fixed at a temperature-specified value given by the database presented in [36]. As a result, the fitting routine was performed iteratively for each transition with an updated Doppler width, and narrowing parameter if applicable, corresponding to the temperature given by the two-color ratio of integrated absorbances. After two iterations, the temperature converged within 2 %. This approach was validated in controlled static cell experiments discussed in Sect. 5. Once the fitting routine converged, $\overline{T}_{n_i}$ and N_i were calculated from the integrated absorbances returned by the fitting routine, as discussed in Sect. 3.1. It is worth noting that when the gas conditions
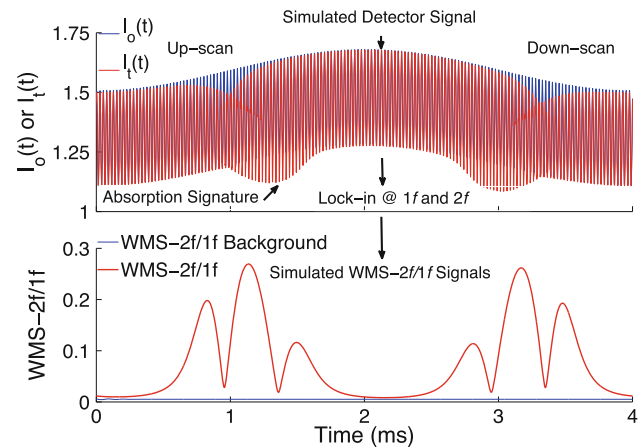

Fig. 3 Simulated detector signal (*top*) and corresponding WMS-2f/1f signal (*bottom*) for a single TDL scanned over an H$_2$O absorption feature at 500 Hz

are nonuniform along the LOS, the lineshape parameters inferred from the best-fit WMS-2f/1f spectrum are simply numerical artifacts that enable the lineshape function of choice to match the actual lineshape and recover the integrated absorbance.

In the spectral-fitting routine, WMS signals were simulated according to the methodology put forth by Sun et al. [35] that properly accounts for all forms of intensity tuning and is valid for all optical depths, modulation depths, and scan amplitudes. In this method, the time-varying incident laser intensity, $I_o(t)$, is measured or simulated for each laser and the time-varying optical frequency, $v(t)$, is simulated after characterization with an etalon. The time-varying transmitted laser intensity, $I_t(t)$ given by (7), is then simulated using Beer's law with the measured or simulated $I_o(t)$, the simulated $v(t)$, and an absorption spectrum model. After simulating $I_t(t)$, simulated WMS signals are then extracted from the simulated $I_t(t)$ using a digital lock-in filter. Figure 3 shows an example simulated detector signal [$I_o(t)$ and $I_t(t)$] and corresponding scanned-WMS-2f/1f signals for a single laser scanned over an H$_2$O transition.

$$I_t(t) = I_o(t) \exp[-\alpha(v(t))]$$
$$= I_o(t) \exp\left[-\sum_j A_j \phi_j(v(t), T, P, \chi)\right] \quad (7)$$

4 Line selection and evaluation

4.1 Line selection

To provide high signal-to-noise ratio (SNR) over the measurement domain, three water vapor transitions in the

Table 1 Relevant spectroscopic parameters for the H_2O transitions used

Line	v_o (cm^{-1})	E'' (cm^{-1})	S(296 K) (cm^{-1}/molecule-cm^{-2})	
			Measured/(uncertainty)	HITEMP'10/(uncertainty)
A	3,920.089	704.214	2.56×10^{-20}/(2.1 %)	2.58×10^{-20}/(5–10 %)
B	4,029.524[a]	2,660.945	4.44×10^{-24}/(2.3 %) [36]	4.27×10^{-24}/(5–10 %)
C	4,030.729[a]	4,889.488	1.08×10^{-28}/(2.5 %)	1.16×10^{-28}/(10–20 %)

Linestrengths quoted for doublet transitions are quoted as the sum of the doublet

The linestrength of Lines A and C was measured as done by Goldenstein et al. [36]

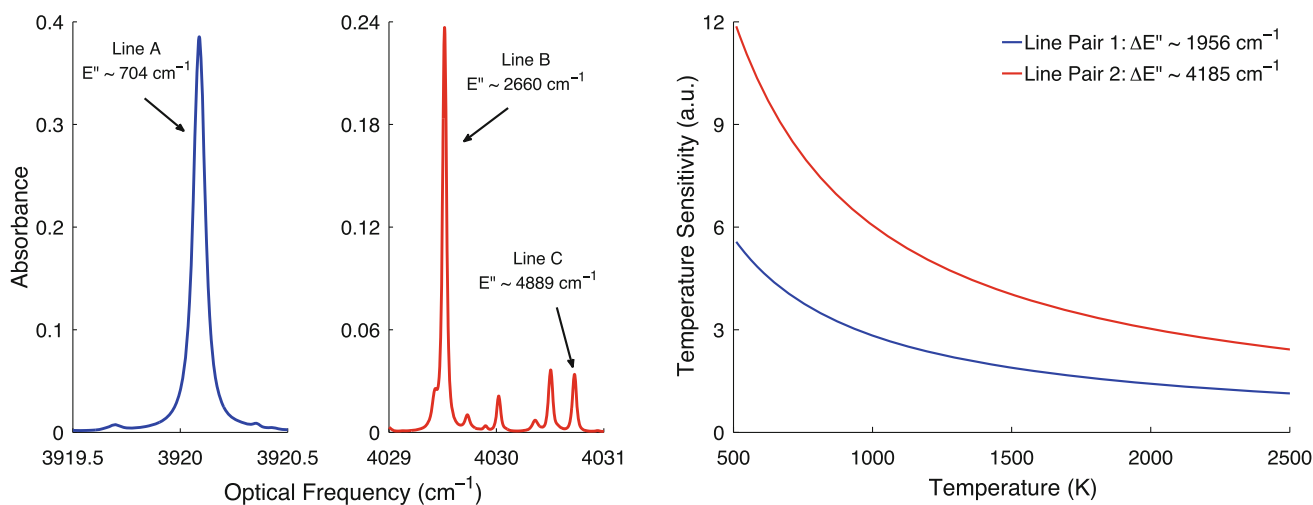v_o and E'' were taken from [38]

[a] Denotes a doublet transition

Fig. 4 Simulated absorbance spectra (*left*) for *Lines A, B,* and *C* at 0.8 bar, 1,500 K, and 10 % H_2O with a path length of 3.8 cm. Temperature sensitivity (*right*) for *line pairs* 1 and 2 as a function of temperature. *Line Pair* 1 = *Lines A* and *B*, *Line Pair* 2 = *Lines A* and *C*

stronger fundamental vibration bands near 2.5 μm were used to measure the gas temperature and H_2O column density throughout the scramjet combustor. The pertinent spectroscopic parameters for these lines, labeled A, B, and C, are given in Table 1. In addition, Fig. 4 (left) shows simulated absorbance spectra for these lines at 0.8 bar, 1,500 K, and 10 % H_2O by mole with a path length of 3.81 cm. Lines A and B (*line pair* 1) were used to characterize the free stream, and Lines A and C (*line pair* 2) were used to characterize the nonuniform reaction zone (shown in Fig. 1). Line B was chosen according to conventional line selection techniques [37], since the gas in the free stream is expected to be near uniform along the LOS. However, Lines A and C were chosen according to the methodology put forth in [21] since the temperature and composition of the gas in the reaction zone are expected to be nonuniform along the LOS. In addition to incorporating conventional line selection rules [37], this method uses two transitions with strengths that scale near-linearly with temperature over the domain of the

temperature nonuniformity to enable accurate determination of $\overline{T}_{n_i}$ and N_i from the integrated absorbance of two transitions.

4.2 Evaluation of chosen lines

4.2.1 Signal strength

To achieve sufficient SNR in harsh environments, strong absorption transitions must be used. The fundamental-vibration-band transitions used here are 1.5–20 times stronger, depending on temperature, than the combination- and overtone-band transitions used in other scramjet sensors [12, 13, 16, 17]. In addition, the reduction in Doppler width associated with using lines near 2.5 μm (as opposed to 1.4 μm) leads to an increase in peak absorbance on the order of 20 % for typical atmospheric pressure flame conditions. As a result, using lines in the fundamental H_2O bands near 2.5 μm provides large gains in signal strength, and thereby, sensor accuracy and precision.

4.2.2 Temperature sensitivity

Large temperature sensitivity is critical to the success of all thermometry techniques. Since the temperature is inferred from the two-color ratio of integrated absorbance, R, temperature sensitivity is defined here as the unit change in R per unit change in temperature. Figure 4 (right) shows the temperature sensitivity of *line pairs* 1 and 2 as a function of temperature. It is well known that the temperature sensitivity scales with the difference in lower-state energies, $\Delta E''$ [39]. As a result, the temperature sensitivity of *line pair* 2 ($\Delta E'' = 4{,}185$ cm^{-1}) is always greater than that of *line pair* 1 ($\Delta E'' = 1{,}956$ cm^{-1}). Furthermore, from 1,000 to 2,500 K, the temperature sensitivity of *line pairs* 1 and 2 decreases from 2.8 to 1.1 and 6 to 2.4, respectively. The temperature sensitivity decreases with increasing temperature due to Boltzmann statistics. In general, a temperature sensitivity greater than one is recommended [37]. That said, both line pairs used here are expected to yield excellent thermometry performance over the experimental domain.

4.2.3 Linearity of linestrength

Using lines with strengths that scale linearly with temperature enables the determination of $\overline{T}_{n_i}$ and N_i in a nonuniform gas [21]. However, in reality, the transition linestrength is a nonlinear function of temperature as shown in (2). As a result, it is important to evaluate the accuracy of the linear-linestrength approximation of the chosen transitions for the expected range of temperatures. This was done by least-squares fitting a line to temperature-specified regions of the linestrength curves given by (2). To remove the influence of the value of $S(T_o)$, all linestrength profiles were normalized to a maximum of 1. Figure 5 shows the maximum error in the linear-linestrength approximation, quantified in terms of percent of the linestrength at the mean temperature, for Lines A and C as a function of the mean temperature. For mean temperatures between 1,300 and 2,000 and a 500 K wide temperature range, the linear-linestrength approximation is accurate to within 1.2–2.6 % of the mean linestrength for Lines A and C. While this error cannot be directly translated to errors in $\overline{T}_{n_i}$ and N_i without knowing how the gas conditions vary along the LOS, the results shown in Fig. 5 suggest that the linear-linestrength approximation is accurate for Lines A and C in the nonuniform reaction zone.

4.2.4 Projected performance in nonuniform reaction zone

A scanned-WMS-2f/1f measurement was simulated for a nonuniform LOS to estimate the accuracy of this sensor in a nonuniform combustor. Figure 6 (left) shows an example
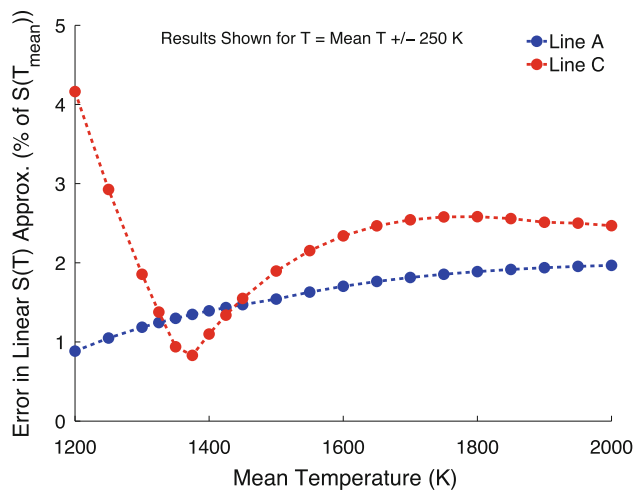

Fig. 5 Maximum error in linear-linestrength approximation for *Lines A* and *C* as a function of mean temperature for a temperature range of 500 K (i.e., ±250 K). The linear-linestrength approximation for *Lines A* and *C* is accurate to within 1.2 and 2.6 % of $S(T_{\text{mean}})$ for mean temperatures between 1,300 and 2,000 K

distribution of temperature and H$_2$O along a simulated optical path. The temperature and H$_2$O mole fraction vary from 1,100 to 1,625 K and 0 to 0.13, respectively, and $\overline{T}_{n_{H_2O}}$ equals 1,450 K. These distribution functions were designed to simulate a case where the measurement LOS passes through two distinct zones of combustion. Figure 6 (right) shows simulated path-integrated WMS-2f/1f spectra and corresponding best fit for Lines A and C. The path-integrated WMS-2f/1f spectra represent a simulated measurement for the LOS shown in Fig. 6 (left) with a uniform pressure of 0.8 bar. In this example, the best-fit spectra match the path-integrated spectra to within less than 0.5 % of the peak signal. The temperature and H$_2$O column density inferred from the best-fit integrated absorbance of Lines A and C agree within 1.5 % of $\overline{T}_{n_{H_2O}}$ and 0.3 % of N_{H_2O}, respectively. To quantify how the accuracy of this sensor varies with mean temperature, these simulations were repeated with $\overline{T}_{n_{H_2O}}$ ranging from 1,200 to 1,900 K in increments of 100 K. The corresponding error in temperature and H$_2$O column density varied from 0.3 to 3.3 % and 0.1 to 2.6 %, respectively. As a result, these simulations indicate that the sensor and data processing methods used are accurate in nonuniform combustion environments with the range of temperatures expected. More details describing how these measurements were simulated can be found in [21].

5 Sensor validation

Scanned-WMS-2f/1f measurements were conducted in air–H$_2$O mixtures within a heated static cell to validate
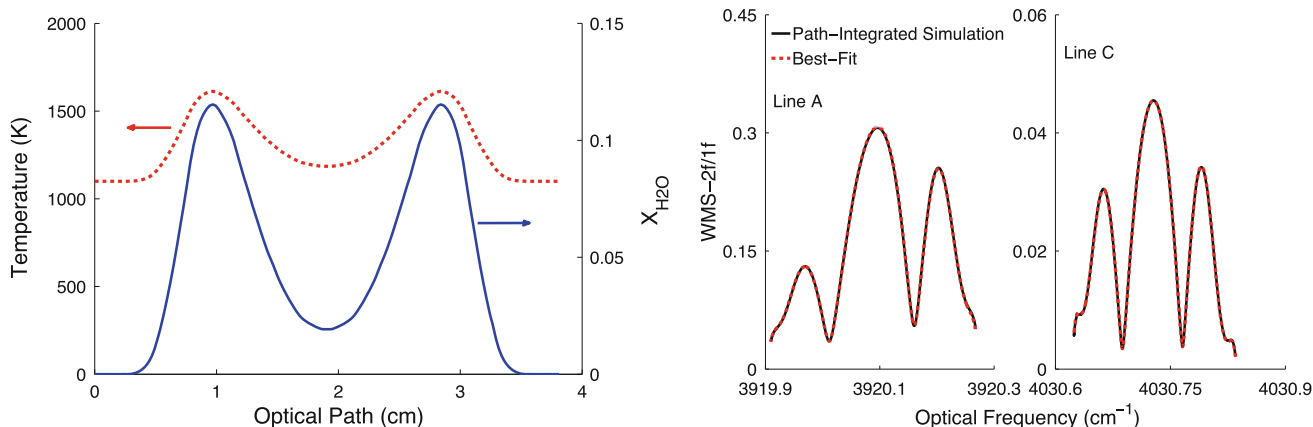
Fig. 6 Example of temperature and H_2O mole fraction distributions used to simulated WMS-2f/1f measurements in a nonuniform reaction zone (*left*). Simulated path-integrated WMS-2f/1f spectra and corresponding best fit for *Lines A* and *C* (*right*). Best-fit spectra recover measured spectra within less than 0.5 % of peak values, and $\overline{T}_{nH_2O}$ and N_{H_2O} to within 1.5 and 0.3 %, respectively
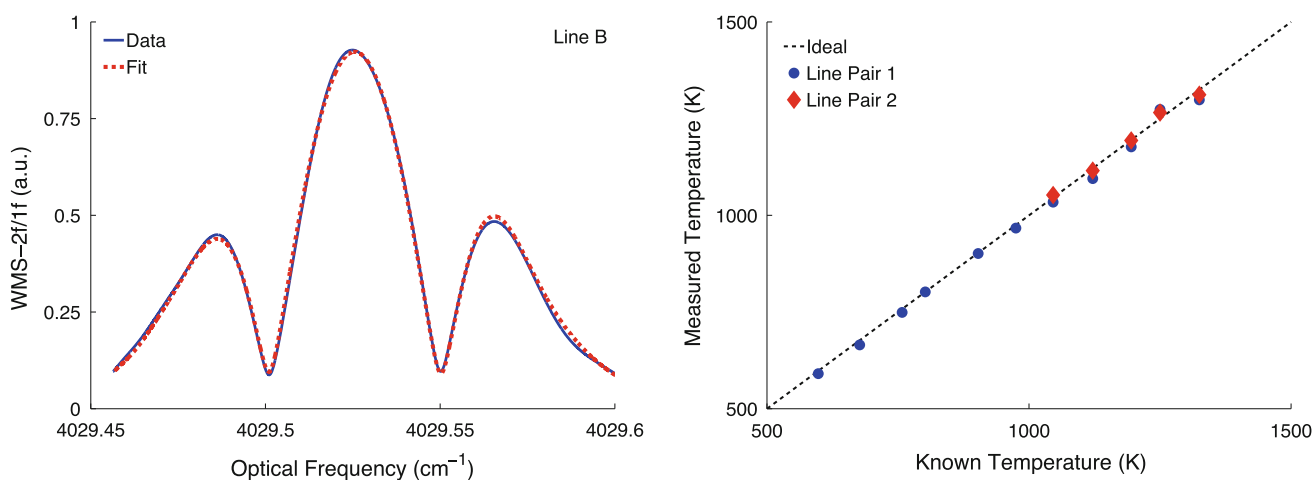

Fig. 7 Scanned-WMS-2f/1f spectrum and corresponding best fit (*left*) for *Line B* in a static cell experiment conducted at 1 bar and 1,000 K with ∼7 % H_2O by mole. Accuracy of scanned-WMS-2f/1f temperature sensor (*right*) using *line pairs* 1 and 2 as a function of temperature for static cell experiments. *Line pairs* 1 and 2 recover the known temperature to within 2 and 1.25 %, respectively. Error bars are too small to be seen. The known temperature was determined from thermocouple measurements

the accuracy of the temperature and H_2O sensor. An experimental setup similar to that shown in Fig. 2 was used in static cell experiments, and more information regarding the furnace and the static cell can be found in [36]. Measurements were conducted with *line pair* 1 from 600 to 1,325 K and with *line pair* 2 from 1,050 to 1,325 K. The gas pressure was 1 bar and the water mole fraction ranged from 1 to 7 % depending on the experiment. The temperature was calculated from the two-color ratio of integrated absorbances inferred from fitting simulated WMS-2f/1f spectra to measured WMS-2f/1f spectra. Figure 7 (left) shows an example of a measured WMS-2f/1f spectrum and corresponding best fit for Line B. The best-fit spectrum recovered the measured WMS-2f/1f spectrum to within 2 % of the peak signal for all lines.

In addition, the 95 % confidence interval (obtained from the fitting routine) in the integrated absorbance was less than ±0.5 % of its best-fit value. Figure 7 (right) shows the temperature-sensing performance of both line pairs. *Line pairs* 1 and 2 recovered the known temperature, measured with thermocouples, to within 2 and 1.25 %, respectively. In addition, the H_2O mole fraction calculated from the integrated absorbance of Line A inferred from scanned-WMS-2f/1f spectral fitting agrees within 2.8 % of that determined from scanned-wavelength direct-absorption measurements. These small differences could result from optical distortion (e.g., etalon reflections) or from differences in the models (e.g., Voigt profile fitting vs. scanned-WMS-2f/1f model) used to convert measured signals to gas properties.

6 Measurements in a model scramjet combustor

This section presents example temperature and H_2O results for Planes I and II (see Fig. 1) of the UVaSCF operating at a global equivalence ratio of 0.15. A more complete discussion of these results and a comparison with LOS absorption measurements of CO and CO_2 conducted in the same facility are given in [40].

Figure 8 shows scanned-WMS-$2f/1f$ time histories for Lines A and C collected inside the cavity flameholder (Plane I, $y = 34.5$ mm). The WMS-$2f/1f$ signal differs (for identical gas conditions) for the up-scan and down-scan since the phase-shift between the laser intensity and optical
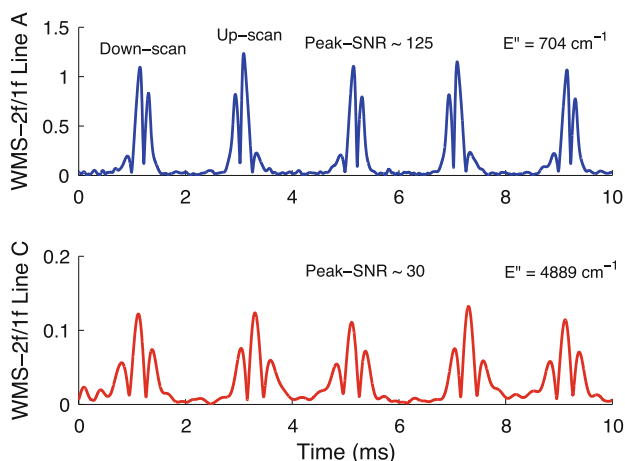
frequency is greater than π. For each half-scan (up-scan or down-scan), a simulated WMS-$2f/1f$ spectrum was least-squares fit to a measured WMS-$2f/1f$ spectrum to determine the integrated absorbance of each transition. Figure 9 shows examples of measured and corresponding best-fit WMS-$2f/1f$ spectra for Lines A and C. The WMS-$2f/1f$ spectrum for Line A is asymmetric due to its large absorbance, and thus asymmetric $1f$ signal [35]. For both lines, the best-fit spectra match the measured spectra to within less than 2 % of the peak signal, which indicates that the fitting routine produced an accurate representation of the experiment. Furthermore, the 95 % confidence interval (obtained from the fitting routine) in the integrated absorbance was less than ±2.5 % of the best-fit value.

$\overline{T}_{n_{H_2O}}$ was calculated by comparing the two-color ratio of integrated absorbances with the two-color ratio of line-strengths. N_{H_2O} was calculated according to (6) using the integrated absorbance of Line A. Figure 10 shows a 0.5-s time history (acquired uninterrupted) of $\overline{T}_{n_{H_2O}}$ and $N_{H_2O} \times \overline{T}_{n_{H_2O}}$ for $y = 28.5$ mm at Plane I. N_{H_2O} was scaled by $\overline{T}_{n_{H_2O}}$ to highlight oscillations in composition. Figure 10 indicates that the gas conditions are nominally steady; however, some low-frequency [O(100 Hz)] oscillations exist, particularly between 0 and 0.3 s. These oscillations in temperature and H_2O are correlated which suggests that the oscillations reflect fluctuations in either the combustion progress or in the transport of combustion products to the measurement location. Similar oscillations were observed throughout the reaction zone.

Figure 11 shows the mean temperature and H_2O column density as a function of y for Planes I and II (see Fig. 1). All measurements were acquired without shutting down the UVaSCF. The bars indicate the temporal variation (1 SD).

Fig. 8 Example scanned-WMS-$2f/1f$ time histories for *Lines A* (*top*) and *C* (*bottom*) acquired in the UVaSCF cavity flameholder ($y = 34.5$ mm on Plane I). Each scanned-WMS-$2f/1f$ spectrum yields a measured temperature and H_2O column density. A total of 500 ms of data were collected at each measurement location
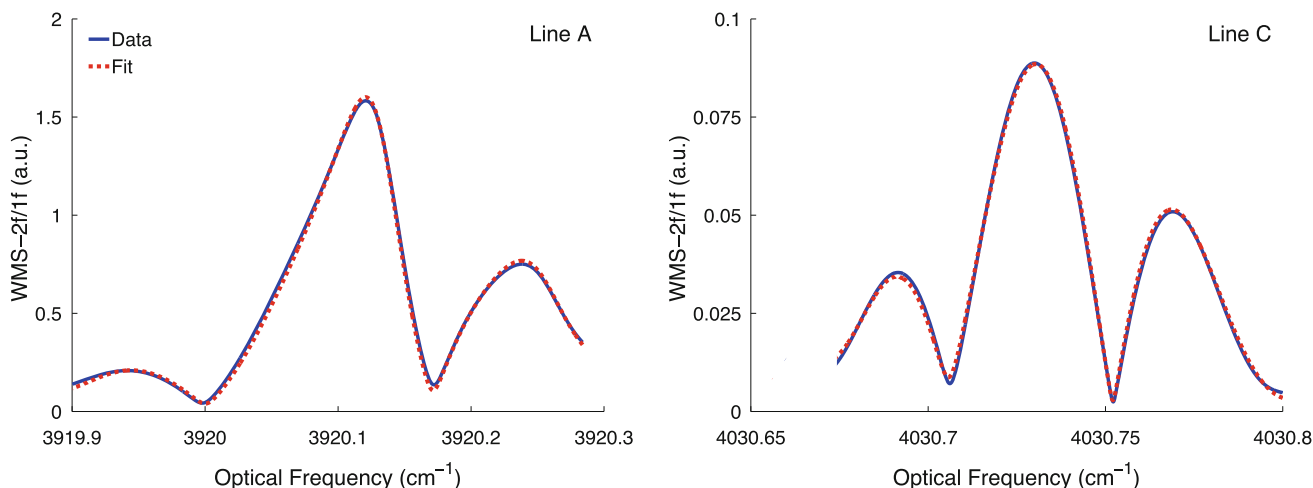

Fig. 9 Examples of measured and best-fit scanned-WMS-$2f/1f$ spectra for *Lines A* (*left*) and *C* (*right*) acquired in the UVaSCF. The best-fit spectra match the measured spectra to within 2 % of the peak signals

The measurement uncertainty, obtained from the 95 % confidence interval in the integrated absorbance of each transition, is typically 5 times smaller than the temporal variation. While pressure measurements are not needed to determine $\overline{T}_{n_{H_2O}}$ or N_{H_2O}, it is worth noting that the static pressure at Planes I and II was approximately 0.73 and 0.83 bar. Figure 11 (left) shows results spanning the entire flow path for Plane I. The temperature first rises away from the cavity wall and then falls monotonically outside the cavity before plateauing at the free-stream temperature near 1,000 K. The H_2O column density, however, falls near
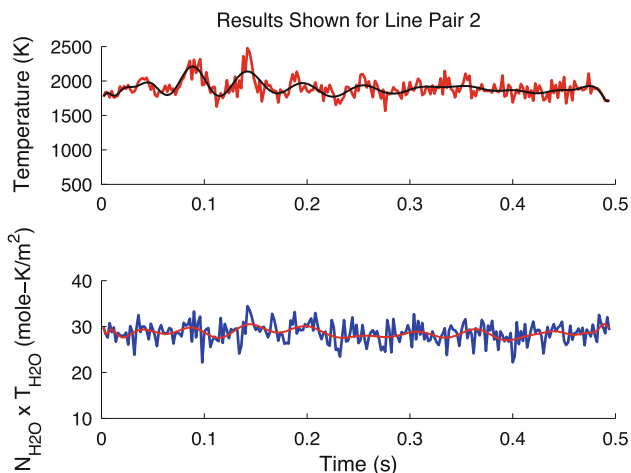
monotonically away from the cavity wall before reaching the expected free-stream value corresponding to 0.8 % H_2O by mole. This immediate drop in column density cannot be explained by the density decrease associated with the rising temperature. As a result, these results suggest that combustion is most complete near the cavity wall and that the lower temperatures could result from three potential sources: (1) heat transfer to the cooled walls (2) increased dilution with cooler gases and (3) thermal stratification in the unburnt gas entering the cavity.

Several interesting conclusions can be made by comparing temperature and H_2O results between Planes I and II. (1) Combustion products penetrate into the free stream a greater distance as the flow moves downstream. Similar results were observed in [16] for a different combustor configuration. (2) Along the expansion wall, the temperature decreases in the flow direction. This could result from heat transfer to the combustor wall. (3) For $y = 21$–27 mm, the H_2O column density increases a large amount from Plane I to II; however, the temperature exhibits a slight decrease. While larger values of H_2O column density suggest greater combustion progress, the minor drop in temperature suggests that the associated heat release is offset by thermal dilution with the free stream. More discussion regarding these results and the performance of the model scramjet combustor can be found in [40].

7 Summary

The design and demonstration of a two-color TDL sensor for temperature and H_2O in an ethylene-fueled scramjet

Fig. 10 Example temperature and H_2O column density time histories acquired in UVaSCF at $y = 28.5$ mm on Plane I. H_2O column density is scaled by temperature to highlight oscillations due to composition only (assuming constant pressure). Smoothed data highlight low-frequency oscillations in temperature and H_2O
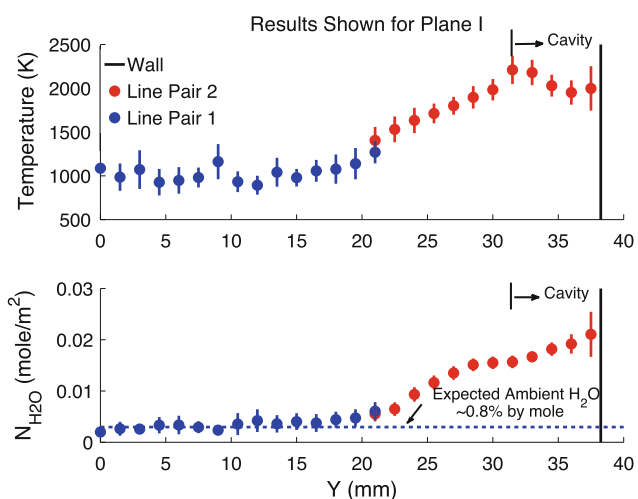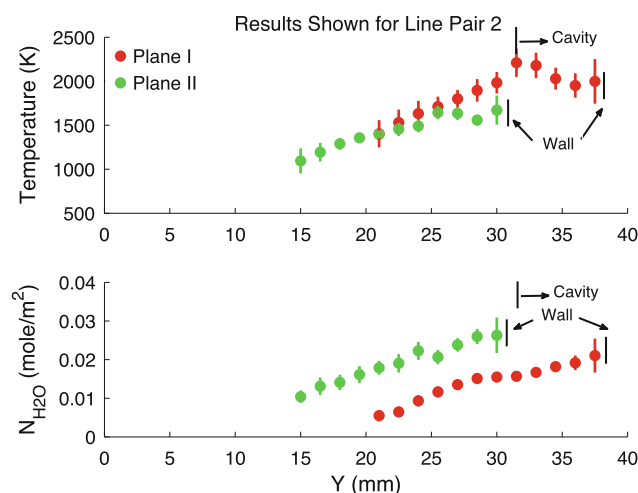

Fig. 11 Time-averaged temperature and H_2O column density measured with *line pairs* 1 and 2 on *Plane I* (*left*) and for *Planes I and II* (*right*). Results are shown for the UVaSCF operating with a global ethylene–air equivalence ratio of 0.17. Outside of the reaction zone,

the WMS sensor recovers the expected H_2O concentration. Inside the reaction zone, the H_2O column density increases between *Planes I and II*, which indicates that combustion progresses in the flow direction

combustor were presented. This sensor used three H_2O transitions in the fundamental vibration bands near 2.5 μm to enable high-SNR measurements in the non-reacting free stream and the ethylene–air reaction zone. The use of fundamental-band transitions enabled three primary advancements over previously used near-infrared-based sensors: (1) up to 20 times larger signals, (2) nearly a factor of two increase in temperature sensitivity, and (3) use of lines with higher lower-state energy for improved measurement fidelity in high-temperature nonuniform flows. In addition, this sensor used a recently developed scanned-WMS-$2f/1f$ spectral-fitting strategy to infer the integrated absorbance of each transition without needing to model the transition linewidths beforehand. This technique enabled accurate line-of-sight WMS absorption measurements of temperature and H_2O in the nonuniform reaction zone.

Temperature and H_2O measurements were presented for more than 35 locations within the UVaSCF combustor. Outside of the reaction zone, the measured H_2O agrees with the expected free-stream value of 0.8 % by mole. Within the reaction zone, low-frequency oscillations in temperature and H_2O were observed. These oscillations indicate fluctuations in either combustion process or transport of combustion products to the measurement location. The measured temperatures were greatest in the middle of the cavity [O(2,100 K)] and decreased away from the cavity before plateauing in the free stream. At a given y-coordinate, the temperature did not change significantly between planes I and II; however, the H_2O column density rose significantly at all locations. These results suggest that the heat release associated with greater combustion progress is offset by dilution with the cooler free stream.

References

1. R.K. Hanson, Applications of quantitative laser sensors to kinetics, propulsion and practical energy systems. Proc. Combust. Inst. **33**, 1–40 (2011)
2. J. Wolfrum, Lasers in combustion: from basic theory to practical devices. Proc. Combust. Inst. 1–41 (1998)
3. M.G. Allen, Diode laser absorption sensors for gas-dynamic and combustion flows. Meas. Sci. Technol. **9**, 545–562 (1998)
4. G.B. Rieker, H. Li, X. Liu, J.T.C. Liu, J.B. Jeffries, R.K. Hanson, M.G. Allen, S.D. Wehe, P.A. Mulhall, H.S. Kindle, A. Kakuho, K.R. Sholes, T. Matsuura, S. Takatani, Rapid measurements of temperature and H_2O concentration in IC engines with a spark plug-mounted diode laser sensor. Proc. Combust. Inst. **31**, 3041–3049 (2007)
5. D.W. Mattison, J.B. Jeffries, R.K. Hanson, R.R. Steeper, S. De Zilwa, J.E. Dec, M. Sjoberg, W. Hwang, In-cylinder gas temperature and water concentration measurements in HCCI engines using a multiplexed-wavelength diode-laser system: sensor development and initial demonstration. Proc. Combust. Inst. **31**, 791–798 (2007)
6. L.A. Kranendonk, J.W. Walewski, T. Kim, S.T. Sanders, Wavelength-agile sensor applied for HCCI engine measurements. Proc. Combust. Inst. **30**, 1619–1627 (2005)
7. S.T. Sanders, D.W. Mattison, J.B. Jeffries, R.K. Hanson, Time-of-flight diode-laser velocimeter using a locally seeded atomic absorber: application in a pulse detonation engine. Shock Waves **12**, 435–441 (2003)
8. D.W. Mattison, M.A. Oehlschlaeger, C.I. Morris, Z.C. Owens, E.A. Barbour, J.B. Jeffries, R.K. Hanson, Evaluation of pulse detonation engine modeling using laser-based temperature and OH concentration measurements. Proc. Combust. Inst. **30**, 2799–2807 (2005)
9. A.W. Caswell, S. Roy, X. An, S.T. Sanders, F.R. Schauer, J.R. Gord, Measurements of multiple gas parameters in a pulsed-detonation combustor using time-mode-locked lasers. Appl. Opt. **52**, 2893–2904 (2013)
10. R.M. Spearrin, C.S. Goldenstein, J.B. Jeffries, R.K. Hanson, in *29th International Symposium on Shock Waves*. Mid-infrared laser absorption diagnostics for detonation studies (Madison, 2013)
11. C.S. Goldenstein, I.A. Schultz, R.M. Spearrin, J.B. Jeffries, K. Hanson, in *24th International Colloquium on the Dynamics of Explosions and Reactive Systems*. Diode laser measurements of temperature and H_2O for monitoring pulse detonation combustor performance (Taiwan, 2013)
12. J.T.C. Liu, G.B. Rieker, J.B. Jeffries, M.R. Gruber, C.D. Carter, T. Mathur, R.K. Hanson, Near-infrared diode laser absorption diagnostic for temperature and water vapor in a scramjet combustor. Appl. Opt. **44**, 6701–6711 (2005)
13. A.D. Griffiths, A.F.P. Houwing, Diode laser absorption spectroscopy of water vapor in a scramjet combustor. Appl. Opt. **44**, 6653–6659 (2005)
14. C.L. Strand, R.K. Hanson, in *47th AIAA/ASME/SAE/ASEE Joint Propulsion Conference & Exhibit*. Thermometry and velocimetry in supersonic flows via scanned wavelength-modulation absorption spectroscopy (American Institute of Aeronautics and Astronautics, 2011) AIAA 2011-5600
15. L.S. Chang, J.B. Jeffries, R.K. Hanson, Mass flux sensing via tunable diode laser absorption of water vapor. AIAA J **48**, 2687–2693 (2010)
16. I.A. Schultz, C.S. Goldenstein, J.B. Jeffries, R.K. Hanson, R.D. Rockwell, C.P. Goyne, TDL absorption sensor for in situ determination of combustor progress in scramjet combustor ground testing. J. Propuls. Power (2014) (in press)
17. F. Li, X. Yu, W. Cai, L. Ma, Uncertainty in velocity measurement based on diode-laser absorption in nonuniform flows. Appl. Opt. **51**, 4788–4797 (2012)
18. K.H. Lyle, J.B. Jeffries, R.K. Hanson, M. Winter, Diode-laser sensor for air-mass flux 2: non-uniform flow modeling and aeroengine tests. AIAA J **45**, 2213–2223 (2007)
19. L.A. Kranendonk, A.W. Caswell, C.L. Hagen, C.T. Neuroth, D.T. Shouse, J.R. Gord, S.T. Sanders, Temperature measurements in a gas-turbine-combustor sector rig using swept-wavelength absorption spectroscopy. J. Propuls. Power **25**, 859–863 (2009)
20. L. Ma, X. Li, S.T. Sanders, A.W. Caswell, S. Roy, D.H. Plemmons, J.R. Gord, 50-kHz-rate 2D imaging of temperature and H_2O concentration at the exhaust plane of a J85 engine using hyperspectral tomography. Opt. Express **21**, 1152–1162 (2013)

21. C.S. Goldenstein, I.A. Schultz, J.B. Jeffries, R.K. Hanson, Two-color absorption spectroscopy strategy for measuring the column density and path average temperature of the absorbing species in nonuniform gases. Appl. Opt. **52**, 7950 (2013)

22. L. Hildebrandt, R. Knispel, S. Stry, J.R. Sacher, F. Schael, Antireflection-coated blue GaN laser diodes in an external cavity and Doppler-free indium absorption spectroscopy. Appl. Opt. **42**, 2110–2118 (2003)

23. C.S. Goldenstein, C.L. Strand, I.A. Schultz, K. Sun, J.B. Jeffries, R.K. Hanson, Fitting of calibration-free scanned-wavelength-modulation spectroscopy spectra for determination of gas properties and absorption lineshapes. Appl. Opt. **53**, 356–367 (2014)

24. L.S. Rothman, I.E. Gordon, A. Barbe, D.C. Benner, P.F. Bernath, M. Birk, V. Boudon, L.R. Brown, A. Campargue, J.P. Champion, K. Chance, L.H. Coudert, V. Dana, V.M. Devi, S. Fally, J.M. Flaud, R.R. Gamache, A. Goldman, D. Jacquemart, I. Kleiner, N. Lacome, W.J. Lafferty, J.-Y. Mandin, S.T. Massie, S.N. Mikhailenko, C.E. Miller, N. Moazzen-Ahmadi, O.V. Naumenko, A.V. Nikitin, J. Orphal, V.I. Perevalov, A. Perrin, A. Predoi-Cross, C.P. Rinsland, M. Rotger, M. Šimečková, M.A.H. Smith, K. Sung, S.A. Tashkun, J. Tennyson, R.A. Toth, A.C. Vandaele, J. Vander Auwera, The HITRAN 2008 molecular spectroscopic database. J. Quant. Spectrosc. Radiat. Transf. **110**, 533–572 (2009)

25. J.A. Silver, Frequency-modulation spectroscopy for trace species detection: theory and comparison among experimental methods. Appl. Opt. **31**, 707–717 (1992)

26. D.S. Bomse, A.C. Stanton, J.A. Silver, Frequency modulation and wavelength modulation spectroscopies: comparison of experimental methods using a lead-salt diode laser. Appl. Opt. **31**, 718–731 (1992)

27. P. Kluczynski, O. Axner, Theoretical description based on Fourier analysis of wavelength-modulation spectrometry in terms of analytical and background signals. Appl. Opt. **38**, 5803–5815 (1999)

28. H. Li, G.B. Rieker, X. Liu, J.B. Jeffries, R.K. Hanson, Extension of wavelength-modulation spectroscopy to large modulation depth for diode laser absorption measurements in high-pressure gases. Appl. Opt. **45**, 1052–1061 (2006)

29. G.B. Rieker, J.B. Jeffries, R.K. Hanson, Calibration-free wavelength-modulation spectroscopy for measurements of gas temperature and concentration in harsh environments. Appl. Opt. **48**, 5546–5560 (2009)

30. L.C. Philippe, R.K. Hanson, Laser diode wavelength-modulation spectroscopy for simultaneous measurement of temperature, pressure, and velocity in shock-heated oxygen flows. Appl. Opt. **32**, 6090–6103 (1993)

31. T. Fernholz, H. Teichert, V. Ebert, Digital, phase-sensitive detection for in situ diode-laser spectroscopy under rapidly changing transmission conditions. Appl. Phys. B Lasers Opt. **75**, 229–236 (2002)

32. R.T. Wainner, B.D. Green, M.G. Allen, M.A. White, J. Stafford-Evans, R. Naper, Handheld, battery-powered near-IR TDL sensor for stand-off detection of gas and vapor plumes. Appl. Phys. B Lasers Opt. **75**, 249–254 (2002)

33. V. Ebert, H. Teichert, P. Strauch, T. Kolb, H. Seifert, J. Wolfrum, Sensitive in situ detection of CO and O_2 in a rotary kiln-based hazardous waste incinerator using 760 nm and new 2.3 μm diode lasers. Proc. Combust. Inst. **30**, 1611–1618 (2005)

34. D.T. Cassidy, J. Reid, Atmospheric pressure monitoring of trace gases using tunable diode lasers. Appl. Opt. **21**, 1185–1190 (1982)

35. K. Sun, X. Chao, R. Sur, C.S. Goldenstein, J.B. Jeffries, R.K. Hanson, Analysis of calibration-free wavelength-scanned modulation spectroscopy for practical gas sensing using tunable diode lasers. Meas. Sci. Technol. **24**, 12 (2013)

36. C.S. Goldenstein, J.B. Jeffries, R.K. Hanson, Diode laser measurements of linestrength and temperature-dependent lineshape parameters of H_2O-, CO_2-, and N_2-perturbed H_2O transitions near 2474 and 2482 nm. J. Quant. Spectrosc. Radiat. Transf. **130**, 100–111 (2013)

37. X. Zhou, J.B. Jeffries, R.K. Hanson, Development of a fast temperature sensor for combustion gases using a single tunable diode laser. Appl. Phys. B **81**, 711–722 (2005)

38. L.S. Rothman, I.E. Gordon, R.J. Barber, H. Dothe, R.R. Gamache, A. Goldman, V.I. Perevalov, S.A. Tashkun, J. Tennyson, HITEMP, the high-temperature molecular spectroscopic database. J. Quant. Spectrosc. Radiat. Transf. **111**, 2139–2150 (2010)

39. A. Farooq, J.B. Jeffries, R.K. Hanson, In situ combustion measurements of H_2O and temperature near 2.5 μm using tunable diode laser absorption. Meas. Sci. Technol. **19**, 075604 (2008)

40. I.A. Schultz, C.S. Goldenstein, M. Spearrin, J.B. Jeffries, R.K. Hanson, Multispecies mid-infrared absorption measurements in a hydrocarbon-fueled scramjet combustor. J. Propuls. Power. (2014)